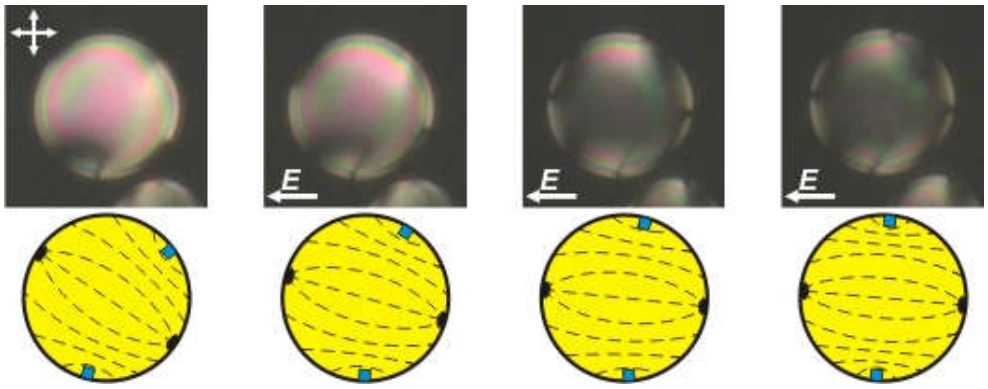
E
E
E

Director configurations in nematic droplets with tilted surface anchoring

Mikhail Nikolaevich Krakhalev[a,b], Oxana Olegovna Prishchepa[a,b], Vitaly Sergeevich Sutormin[a] and Victor Yakovlevich Zyryanov[a]

[a]*Kirensky Institute of Physics, Krasnoyarsk Scientific Center, Siberian Branch, Russian Academy of Sciences, Krasnoyarsk 660036, Russia;* [b]*Siberian Federal University, Krasnoyarsk 660041, Russia*

Corresponding author: M.N. Krakhalev, e-mail: kmn@iph.krasn.ru

Director configurations in nematic droplets with tilted surface anchoring

The polymer dispersed nematic liquid crystal with the tilted surface anchoring has been studied. The droplet orientational structures with two point surface defects-boojums and the surface ring defect are formed within the films. The director tilt angle $\alpha = 40° \pm 4°$ at the droplet interface and LC surface anchoring strength $W_s \sim 10^{-6}$ (J m^{-2}) have been estimated. The bipolar axes within the studied droplets of oblate ellipsoidal form can be randomly oriented are oriented randomly relatively to the ellipsoid axes as opposed to the droplets with homeotropic and tangential anchoring.

Keywords: polymer dispersed liquid crystal, nematic droplet, director configuration, boundary conditions, surface anchoring strength, optical texture

1. Introduction

Polymer dispersed liquid crystals (PDLCs) are polymer films with dispersed liquid crystals (LC) droplets. The orientational structure (director configuration) in LC droplets is specified by the surface anchoring and other material parameters. The optical properties of the films depend on the director configuration inside LC droplets, the film morphology (form, size and arrangement of the droplets) and the ratio of LC and polymer refractive indices. Electric or magnetic field can transform the LC orientational structure, this changes the macroscopic optical properties of PDLC films. For example, when the ordinary refractive index ($n_\perp$) of LC with positive dielectric constant is close to the refractive index of polymer (n_p), the electric field applied perpendicular to the film plane switches the PDLC film from the scattering state into the transparent one [1-5]. At present, there have been well investigated PDLC films containing the nematic droplets with the most common configurations: bipolar for strong tangential anchoring, radial for strong homeotropic anchoring [6-8] and axial for strong homeotropic or weak anchoring [9-11]. At weak anchoring, the elastic deformation energy of director can

decrease within bulk due to the director deviation from its orientation assigned by the polymer wall at a part of the interface. This sometimes results in the formation of the defect-less axial structure [9, 12, 13]. The droplets with the homogeneous tilted boundary conditions were observed infrequently. So, LC droplets with homogeneous tilted anchoring, which are formed from the isotropic phase and coexist in parallel with it, were observed in [14, 15]. A similar case was for the nematics dispersed in the liquid matrixes doped with the surfactants. The tilted anchoring was realized within liquid matrix in the certain temperature range at the constant concentration of surfactant [7] or for the certain range of surfactant concentration [16]. In PDLC films the resultant director orientation at the interface depends on the droplet size [9], the length of lateral alkyl chains of polymer macromolecules [12], the temperature [17], the variation of curing agent of photo-curable polymer [18], the surfactant content in polymer matrix or LC [19, 20].

The present paper describes the results of experimental investigation of the director configurations within the nematic droplets dispersed in the polymer matrix with the homogeneous tilted anchoring at the interface.

2. Experimental approach

There have been investigated PDLC films based on the poly(isobutyl methacrylate) (PiBMA) (Aldrich) and nematic mixture LN-396 (Belarusian State Technological University) consisting of 40% 4-n-pentyl-4'-cyanobiphenyl (5CB), 20 % 4'-propoxy-biphenyl-4-carbonitrile (3OCB), 15 % 4'-butoxy-biphenyl-4-carbonitrile (4OCB), 18 % 4-Butyl-cyclohexanecarboxylic acid 4-ethoxy-phenyl ester (4CEPO2), 7 % 4-Butyl-cyclohexanecarboxylic acid 3'-methyl-4'-pentyl-biphenyl ester (by weight).

For this mixture the melting temperature is T_m = -20°C, the clearing point is T_c = +66°C. At the temperature T = +22 C the refractive indices of LC (λ = 0.589) are $n_{\|}$ = 1.69, $n_{\perp}$ = 1.52, anisotropy of dielectric conductivity is Δε = 10.2. The refractive index of polymer is n_p = 1.477. The samples were made by SIPS (solvent induced phase separation) technique [1]. LC was added to the 4 % solution of polymer and toluene. The weight ratio of the components was LN-396 : PiBMA = 60 : 40. To create the electro-optical cell, the prepared homogeneous solution was poured on the glass substrate with ITO electrodes separated by 410 μm gap from each other (Figure 1) and was dried during 24 hours. In the result, the PDLC film containing the monolayer arranged LC droplets was formed. The droplets size (droplet diameter in the film plane) was in the range 7-30 μm. The average thickness of the film in the central part was 35 μm.

The optical textures of the nematic droplets were examined by the polarizing optical microscope (POM) Axio Imager.A1m (Carl Zeiss). After the phase separation, a part of LC remains in the polymer (LC : PiBMA = 25 : 75). It plasticizes the polymer matrix and changes its electric and optical parameters [1]. Namely, the refractive index of polymer matrix increases and gets almost equal to the LC refractive index $n_{\perp}$. Being observed without analyzer the interface is practically invisible where the director is aligned perpendicular to the light polarization because $n_{\perp} \cong n_p$. And vice versa, it is sharply seen where the director is parallel to the polarizer orientation [19-20]. Thus, the comprehensive analysis of the optical textures in both crossed polarizers [1, 21] and without analyzer allows determining the director distribution within the droplet.

The PDLC cell design permits to watch the variation of LC optical textures under the action of the electric field applied along the film plane. We used the G3-123

generator which makes the ac 1kHz voltage varied in the range 0-200 V (RMS) and measured by APPA-301 digital multimeter.

Another sandwich-like cell with LC layer was made to determine the surface anchoring strength at the LC-polymer interface. The mixture of PiBMA (75%) and LC LN-396 (25%) was used as the orienting layers at the inner sides of the cell substrates. These layers were formed from the toluene solution by the centrifuge method without further treatment. The cell gap was 13 μm. The cell was filled with LC by the capillary method at room temperature.

3. Results and discussion

3.1. Optical textures and orientational structures of nematic droplets

It is known that PiBMA specifies the homeotropic boundary conditions for both the E7 nematic mixture [22] and the EN18 nematic mixture-based cholesteric [23]. In the studied PDLC films based on LN-396 and PiBMA the droplet textures (Figure 2) differ significantly from those ones which are proper to both the homeotropic anchoring (radial, axial, escaped radial structures) and the planar one (bipolar, twist-bipolar, toroidal configurations).

Figure 3 shows the optical textures of the droplet (see Figure 2(a)) at some turning angles of the sample relative to the polarizers. Four topological features dividing the droplet circle into four equal arcs are observed without analyzer (Fig. 3a, bottom). Top and bottom features are connected by the dark line. At that, the droplet border is clearly seen over all the circle. This indicates that the director is oriented mostly in parallel to the polarizer. A vertical thin extinction band connecting the top and bottom features at the border and a horizontal extinction band connecting two other features are seen in crossed polarizers (Figure 3(a), top). Besides, there appear four extinction areas

located close to the droplet circle and approximately equidistant from the vertical and horizontal extinction lines.

The sample rotation by 45° clockwise relative to the polarizers changes completely the optical texture observed in both crossed polarizers and without analyzer (Figure 3(b)). The interference color pattern without extinction bands is seen in crossed polarizers. Four identical sections along the droplet border are seen without analyzer. When moving around the droplet clockwise, the maximum darkening is revealed in the feature areas. Then the border sharpness decreases gradually to the next feature.

The optical texture analogous to the one presented in Figure 3(a) is observed in crossed polarizers when the sample is turned at 90° relative to the polarizers (Figure 3(c)). When the analyzer is off, the droplet border loses its clearness.

When scanning the extinctions bands (Figure 3, top row) and taking into account the preferable director orientation at the droplet border (Figure 3, bottom row), an anchoring α angle between the $\boldsymbol{n}$ director and the $\boldsymbol{N}$ normal to the surface can be estimated (Figure 3(d)). The director may be parallel to either the horizontal or vertical polarizer in the extinction area located on the left bottom (Figure 3(a), top). However observing the droplet without analyzer shows that the director has approximately horizontal orientation here (Figure 3(d)). The angle thus estimated at various points of the interface, except the features neighborhood, is $\alpha = 40° \pm 4°$.

The α angle invariance along the droplet circle allows drawing schematically the orientational structure in the main droplet section by the film plane (Figure 3(d)). Such a pattern of director field distribution corresponds to the structure with two point surface defects-boojums and the ring surface defect, which was observed earlier in the liquid matrixes [7, 14, 15]. The section of the ring defect by the film plane reveals as two

features at the droplet border. The bipolar axis connecting the boojums is the symmetry axis of the orientational droplet structure.

In the PDLC samples under study the optical textures shown in Figure 3 were observed only within the 10 μm droplets and smaller size. Analogous structure with two boojums and the ring surface defect is revealed within the droplets of bigger size (Figure 2(b)), but the extinction bands in the central droplet part is absent for any orientation of the bipolar axis relative to the crossed polarizers. This is typical for the twisted orientational structure within the droplet. A twist angle, determined as azimuthal angle θ between the orientation of bipolar axis and the director orientation at the droplet interface in the equatorial plane, was estimated by the method described in detail in [24]. If Mauguin's condition is satisfied, then light passed through the droplet in crossed polarizers will be quenched simultaneously fulfilling the next requirements: 1) the droplet bipolar axis is aligned perpendicularly to the observing direction; 2) the polarizer orientation is perpendicular (or parallel) to the director projection at the bottom droplet surface; 3) the analyzer orientation is parallel (or perpendicular) to the director projection at the top droplet surface. It is the twist angle at which the director orientation in the central part is parallel to the bipolar axis, must be selected out of two possible ones. For these droplets with two boojums and ring defect, it means that the bipolar axis must be within the film plane and the plane of the ring defect must be perpendicular to the film plane. The twist angle measured by the method (Figure 4) for the various droplets satisfying to the above-mentioned conditions depends on the droplet size. So for the droplets of 10 μm diameter the twist angle is $\theta = 12^{\circ} \pm 3^{\circ}$ and for the droplets of 21 μm diameter $\theta = 27^{\circ} \pm 3^{\circ}$.

Apart from the above-described droplet textures, the other ones are also observed (Figure 2(c)). Turning the sample relative to polarizers leads to the

complicated change of the droplet texture in both crossed polarizers and without analyzer (Figure 5).

The turning angle of the microscopic stage is 0° (Figure 5(a)) when the droplet border is seen less clearly without analyzer. At that, one point defect is revealed. Turning the sample makes the droplet border clearer (Figure 5(b)-(c)). The maximum sharp borders are seen at 90° (Figure 5(d)). Lowering the macroscopic stage, there can be clearly observed the one point defect (Figure 6(a)), the ring defect (Figure 6(b)) and the second point defect (Figure 6(c)).

Analyzing the optical texture we can state that the droplet has the orientational structure with two boojums, ring defect and the bipolar axis tilted to the film plane. The absence of the extinction bands indicates the presence of torsion deformation as in the case of Figure 2(b) and Figure 4. The angle between the bipolar axis and the film plane is may be varied from 0° (Figure 2(a),(b)) to the approximate 90° (Figure 2(d)) in the droplet ensemble. If the bipolar axis is orthogonal to the film plane, the optical texture does not depend on the turning of the microscope stage.

The droplet shown in Figure 2(e) has two boojums and the ring defect as well. Figure 7 presents the images of this droplet at the various angles of the bipolar axis orientation relative to the polarizer. It should be noted that the plane of ring defect removes from the droplet centre to one of the boojums. At that, the torsion deformation occurs within the droplet. Such structures are usually observed within large droplets (more 15 μm). The displacement of the ring defect can be various within different droplets.

3.2. Surface anchoring strength

Within the samples with tilted boundary conditions, the surface anchoring strength can

be determined by the field-free method which allows analyzing the domain walls of Bloch or Neel formed in the LC layer schlieren-texture [25]. The schlieren-texture, having the point and linear defects, the domain Bloch walls, is formed in the cell produced to determine the surface anchoring strength for the LC and polymer film based on PiBMA (75 %) and LN-396 (25 %). The polar surface anchoring strength W_S can be determined through the measurements of the thickness d of the Bloch's walls:

$$W_S\left(1-\frac{\sin 4\alpha}{2(\pi-2\alpha)}\right)=\frac{h}{d^2}\frac{K_{22}}{2}(\pi-2\alpha)^2,$$

where α is angle between the director and the normal to the interface, h is cell thickness, K_{22} is the elastic constant of the torsion deformation. We measured the cell thickness $h \cong 13$ μm and the Bloch's wall thickness $d \cong 3.0$ μm. The angle $\alpha \cong 40°$ was taken from the measurements in the LC droplets inside the polymer matrix (see above point *3.1*) and $K_{22} \sim 10^{-12}$ (N) [26]. The polar surface anchoring strength was estimated by using these data. It is $W_S \cong 2.4 \cdot 10^6 \cdot K_{22} \sim 10^{-6}$ (J m^{-2}).

3.3. Transformation of the orientational structures under the electric field

The transformation of the director configuration can be observed under the electric field applied along the film plane. What all the droplets have in common is that they are reoriented by bipolar axes along the filed. Small control voltages almost without threshold field are characteristic for the PDLC films under study. For instance, for the experimental cell (Figure 1) the changes of optical patterns are observed practically in all droplets independently of their sizes starting with 20 V voltage. The droplets response to the external electric field reveals in the slow turn (tens seconds) of the whole droplet structure at an angle depending on the applied voltage. The bipolar axes of droplets are aligned entirely along the electric field of 90 V, the planes of ring defects

are oriented perpendicularly to the applied field (Figure 8).

When the bipolar axis is oriented at any angle to the film plane, a similar pattern is observed. If in the initial state the bipolar axis is aligned in the film plane and perpendicularly to the direction of the applied field (Figure 9), the threshold character of reorientation is observed. Visible texture changes appear only at $U_c \cong 40$ V (Figure 9(b),(c)). They are similar to the transformations within the bipolar droplets with rigid planar anchoring [27,28]. Further increasing of the field approximately up to 1.5 U_c leads to the reorientation of bipolar axis close to the field direction (Figure 9(d),(e)).

If the ring defect plane is located asymmetrically relative to the droplet center, the turn of the ring defect and its gradual displacement to the droplet centre occurs simultaneously with reorientation of the bipolar axis under the electric field (Figure 10).

After switching off the electric field, the slow relaxation of the orientational structures into the initial state is observed. The droplets of smaller size take their initial state faster (from tens seconds to tens minutes). The relaxation time of the bigger droplets can take some hours. Some droplets can relax into the states different from the initial one.

4. Conclusions

PDLC films based on the polymer PiBMA and nematic mixture LN-396 have been investigated. The nematic droplets have the orientational structure with two boojums and the ring surface defect. Such orientational structures are formed at the homogeneous tilted anchoring. Similar structures were observed earlier only within LC droplets dispersed in own isotropic phase [14, 15] or in liquid matrix doped with homeotropic surfactant [7, 16]. The tilt angle of the LC director at the interface with polymer has been estimated by the POM method. It is the same for the droplets of different size.

The value of polar surface anchoring strength $W_s \sim 10^{-6}$ (J m^{-2}) was found by using the free-field method. It is by 1-2 orders more than W_s for homologous series of 4-cyano-4'-(*n*-alkyl)biphenyls at the interface with the own isotropic phase [29] where the tilted anchoring was observed. The estimation of the surface extrapolation length $\xi = K / W_{s,}$ where $K = (K_{11} + K_{33}) / 2$, showed that $\xi = (K_{11}+K_{33}) / (4.8\ K_{22}) \sim 1$ μm for the structure under study. In this case the tilted anchoring must be kept over all interface within large droplets (~ 10 μm and more).

It is of great interest that the bipolar axis inside droplets is oriented under various angles relative to the film plane. LC droplets within PDLC are known to look as an oblate ellipsoid [1, 30]. Such a form leads to the orientation of the bipolar droplets symmetric axis along the film plane [1, 31], while the symmetric axis in the axial droplets tends to be oriented perpendicular to the film plane along the short ellipsoid axis [32]. The studied configuration with tilted anchoring has features of both the bipolar structure (central spindle part of droplets close to the bipolar axis) and the axial one (peripheral droplet area). Probably, this peculiarity of the orientational structure provides a small difference of LC energy for various orientations of the bipolar axis relative to the film plane. It can also explain the observed distribution of bipolar axes orientations in the experiment, the small control voltages and longer relaxation time.

Thus, the polymer dispersed nematic liquid crystal films with the tilted boundary conditions have the orientational structure that combines the features of both bipolar and axial configurations. Such features open possibilities to apply these PDLC materials in manufacturing electro-optical devices with the memory effect and the low control voltage. Such features make these PDLC materials prospective for manufacturing electro-optical devices with the memory effect and the low control voltage.

Funding

This work was supported by Russian Foundation for Basic Research (RFBR) under Grants [15-02-06924 and 16-32-00164]; Siberian Branch of the Russian Academy of Sciences (SB RAS) under Complex Program [II.2P 0358-2015-0010]; and V.S.S. acknowledges financial support from RFBR [16-32-60036].

References

[1] Drzaic PS. Liquid Crystal Dispersion. Singapore: World Scientific; 1995.

[2] Kitzerow H-S. Polymer-dispersed liquid crystals. From the nematic curvilinear aligned phase to ferroelectric films. Liq Cryst. 1994;16:1–34.

[3] Doane JW. Polymer dispersed liquid crystal displays. In: Bahadur B, editor. Liquid Crystals–Applications and Uses. Vol. 1. Singapore: World Scientific; 1990. p. 361–395.

[4] Doane JW, Golemme A, West JL, et al. Polymer Dispersed Liquid Crystals for Display Application. Mol Cryst Liq Cryst.1988;165:511–532.

[5] Mucha M. Polymer as an important component of blends and composites with liquid crystals. Prog Polym Sci. 2003;28:837–873.

[6] Candau S, Le Roy P, Debeauvais F. Magnetic Field Effects in Nematic and Cholesteric Droplets Suspended in an Isotropic Liquid. Mol Cryst Liq Cryst. 1972;23:283–297.

[7] Volovik GE, Lavrentovich OD. The topological dynamics of defects: boojums in nematic drops. JETP. 1983;58:1159–1166.

[8] Ondris-Crawford R, Boyko EP, Wagner BG, et al. Microscope textures of nematic droplets in polymer dispersed liquid crystals. J Appt Phys. 1991;69:6380–6386.

[9] Erdmann JH, Žumer S, Doane JW. Configuration Transition in a Nematic Liquid Crystal Confined to a Small Spherical Cavity. Phys Rev Lett. 1990;64:1907–1910.

[10] Goyal RK, Denn MM. Orientational multiplicity and transitions in liquid crystalline droplets. Phys Rev E. 2007;75:021704.

[11] Bodnar VG, Lavrentovich OD, Pergamenshchik VM. The threshold for the hedgehog-ring structural transiton in nematic drops in an alternating electric field. JETP. 1992;74:60–67.

[12] Amundson K, Srinivasarao M. Surface anchoring and electro-optics in polymer-dispersed liquid-crystal films. Mat Res Soc Symp Proc. 1996;425:269–274.

[13] Allender DW, Žumer S. Phase transitions on liquid crystal droplets. Proc SPIE Int Soc Opt Eng. 1989;1080:18–23.

[14] Madhusudana NV, Sumathy KR. Nematic droplets with a new structure. Mol Cryst Liq Cryst. 1983;92(Letters):179–185.

[15] Kim Y-K, Shiyanovskii SV, Lavrentovich OD. Morphogenesis of defects and tactoids during isotropic-nematic phase transition in self-assembled lyotropic chromonic liquid crystals. J Phys Condens Matter. 2013;25:404202.

[16] Gupta JK, Zimmerman JS, de Pablo JJ, et al. Characterization of adsorbate-induced ordering transitions of liquid crystals within monodisperse droplets. Langmuir. 2009;25:9016–9024.

[17] Amundson K. Electro-optic properties of a polymer-dispersed liquid-crystal film: Temperature dependence and phase behaviour. Phys Rev E. 1996;53:2412–2422.

[18] Yan B, He J, Du X, et al. Control of liquid crystal droplet configuration in polymer dispersed liquid crystal with macro-iniferter polystyrene. Liq Cryst. 2009;36:933–938.

[19] Prishchepa OO, Shabanov AV, Zyryanov VYa. Director configurations in nematic droplets with inhomogeneous boundary conditions. Phys Rev E. 2005;72:031712.

[20] Prishchepa OO, Shabanov AV, Zyryanov VYa. Transformation of director configuration upon changing boundary conditions in droplets of nematic liquid crystal. JETP Lett. 2004;79:257–261.

[21] Drzaic PS. Polymer dispersed nematic liquid crystal for large area displays and light valves. J Appl Phys. 1986;60:2142–2148.

[22] Xie A, Higgins DA. Electric-field-induced dynamics in radial liquid crystal droplets studied by multiphoton-excited fluorescence microscopy. Appl Phys Lett. 2004;84:4014–4016.

[23] Kitzerow H-S, Crooker PP. Electric field effects on the droplet structure in polymer dispersed cholesteric liquid crystals. Liq Cryst. 1993;13:31–43.

[24] Drzaic PS. A case of mistaken identity: spontaneous formation of twisted bipolar droplets from achiral nematic materials. Liq Cryst. 1999;26:623–627.

[25] Ryschenkow G, Kleman M. Surface defects and structural transitions in very low anchoring energy nematic thin films. J Chem Phys. 1976;64:404–412.

[26] Demus D, Goodby J, Gray GW, Spiess H-W, Vill V, editors. Fundamentals. Vol. 1, Handbook of liquid crystals. Weinheim: Wiley-VCH; 1998.

[27] Shabanov AV, Presnyakov VV, Zyryanov VYa, et al. Characteristics of the process of reorientation of bipolar drops of a nematic with rigidly fixed poles. JETP Lett. 1998;67:733–737.

[28] Shabanov AV, Presnyakov VV, Zyryanov VYa, et al. Bipolar nematic droplets with rigidly fixed poles in the electric field. Mol Cryst Liq Cryst. 1998;321:245/[689]–258/[702].

[29] Faetti F, Palleschi V. Nematic-isotropic interface of some members of the homologous series of 4-cyano-4'-(*n*-alkyl)biphenyl liquid crystals. Phys Rev A. 1984;30:3241–3251.

[30] Prishchepa OO, Shabanov AV, Zyryanov VYa, et al. Friedericksz threshold field in bipolar nematic droplets with strong surface anchoring. JETP Lett. 2006;84:607–612.

[31] Koval'chuk AV, Kurik MV, Lavrentovich OD, et al. Structural transformations in nematic droplets located in an external electric field. JETP. 1988;67:1065–1073.

[32] Rudyak VYu, Emelyanenko AV, Loiko VA. Structure transitions in oblate nematic droplets. Phys Rev E. 2013;88:052501.

Figure 1. A scheme of electro-optical PDLC cell with the electric field applied along the substrate.

Figure 2. POM images of the typical droplet textures (a)-(e) observed in PDLC based on LN-396 and PiBMA in crossed polarizers (top row) and without analyzer (bottom row). The scale is the same for all images. The orientations of polarizers are marked with double arrows here and in the following figures.

Figure 3. POM images of the LC droplet in crossed polarizers (top row) and without analyzer (bottom row). The bands connecting diametrically opposite features at the border are parallel to the polarizers (a); the sample is turned clockwise relative to the polarizers at 45° angle (b) and at 90°angle (c). The scheme of the proper orientational structure with two boojums (black semicircles) and the ring surface defect (the cross section is indicated by the squares) (d). The bipolar axis is oriented horizontally as in the case (a). α is the anchoring angle between the local director orientation and the normal to interface. The droplet size is 10 μm.

Figure 4. POM images of the LC droplet in crossed polarizers (top row) and without analyzer (bottom row). The bipolar axis of the droplet is perpendicular to the polarizer, the angle between the polarizer and analyzer is 90° (a); the bipolar axis is turned at 20° anticlockwise relative to the polarizer, the angle between the polarizer and analyzer is 130° (b); the scheme of relative orientation of the bipolar axis, the director projection on the picture plane at bottom and top edges (top); the director field over the top droplet surface (bottom) (c). The droplet size is 17 μm.

Figure 5. POM images of the LC droplet in crossed polarizers (top row) and without analyzer (bottom row) at the turning angles of microscopic stage 0° (a), 30° (b), 60° (c), 90° (d). The droplet size is 21 μm.

Figure 6. POM images of the LC droplet shown in Figure 5(b) in crossed polarizers. The objective focuses on the bottom defect-boojum (a), the ring defect (b) and top defect-boojum (c). Single arrows indicate the defect positions.

Figure 7. POM images in crossed polarizers (top row) and without analyzer (bottom row). The bipolar axis is orthogonal to the polarizer (a); the sample is turned at 45°

clockwise relative to the polarizer (b); the sample is turned at 90° clockwise (c). The droplet size is 23 μm.

Figure 8. POM images of the LC droplet in the initial state (a), under the 20 V electric field (b), 50 V (c), 90 V (d) made 1 min after switching the electric field on. Images in crossed polarizers (top row), without analyzer (middle row) and the schemes of the proper droplet structures (bottom row). The droplet size is 9 μm. Here and further, a gap between the electrodes is 410 μm, the direction of the electric field $\boldsymbol{E}$ is shown by a single arrow.

Figure 9. POM images of the LC droplet in the initial state (a) and under the electric field of 40 V (b), 50 V (c), 60 V (d), 90 V (e) made 1 min after switching the electric field on. Images in crossed polarizers (top row), without analyzer (middle row) and the schemes of the proper droplet structures (bottom row). The droplet size is 8 μm.

Figure 10. POM images of the LC droplet in the initial state (a) and under the electric field of 20 V (b), 50 V (c), 90 V (d), made 1 min after switching the electric field on. Images in crossed polarizers (top row), without analyzer (middle row) and the schemes of the proper droplet structures (bottom row). The droplet size is 20 μm.

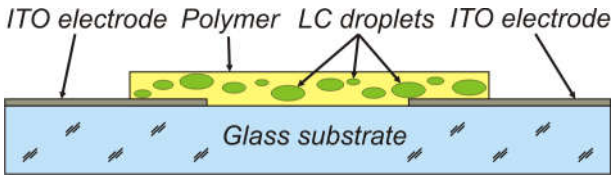

Figure 1. A scheme of electro-optical PDLC cell with the electric field applied along the substrate.

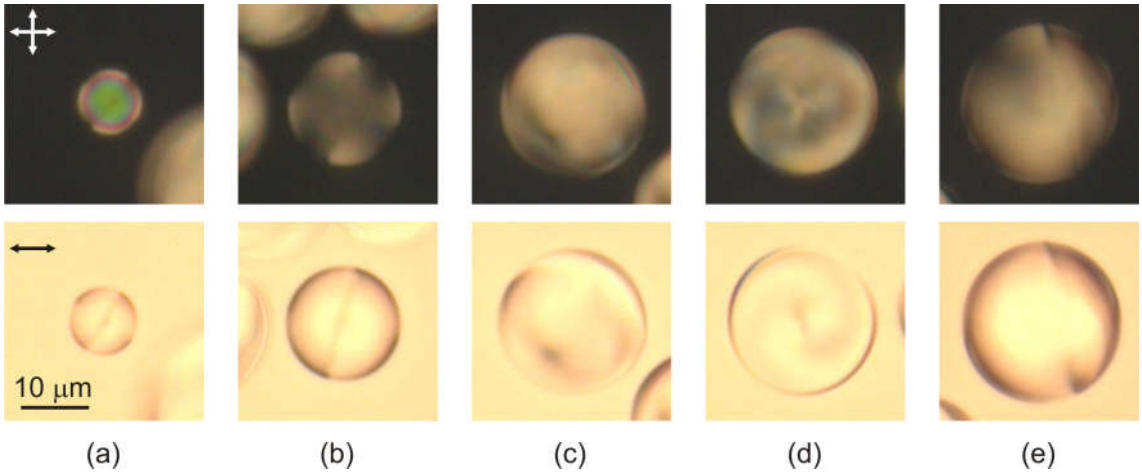

Figure 2. POM images of the typical droplet textures (a)-(e) observed in PDLC based on LN-396 and PiBMA in crossed polarizers (top row) and without analyzer (bottom row). The scale is the same for all images. The orientations of polarizers are marked with double arrows here and in the following figures.

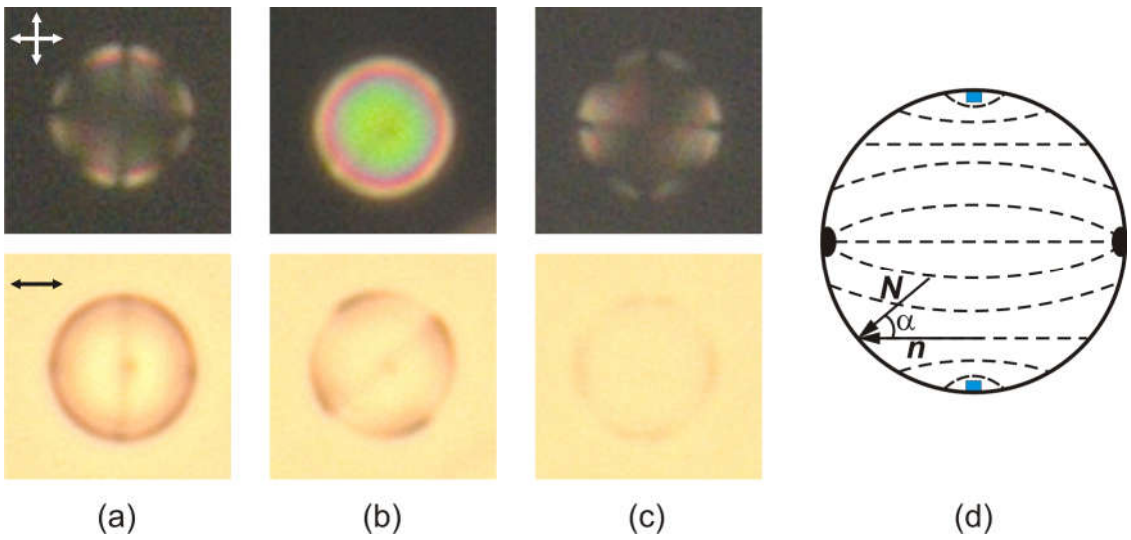

Figure 3. POM images of the LC droplet in crossed polarizers (top row) and without analyzer (bottom row). The bands connecting diametrically opposite features at the border are parallel to the polarizers (a); the sample is turned clockwise relative to the polarizers at 45° angle (b) and at 90°angle (c). The scheme of the proper orientational structure with two boojums (black semicircles) and the ring surface defect (the cross section is indicated by the squares) (d). The bipolar axis is oriented horizontally as in the case (a). α is the anchoring angle between the local director orientation and the normal to interface. The droplet size is 10 μm.

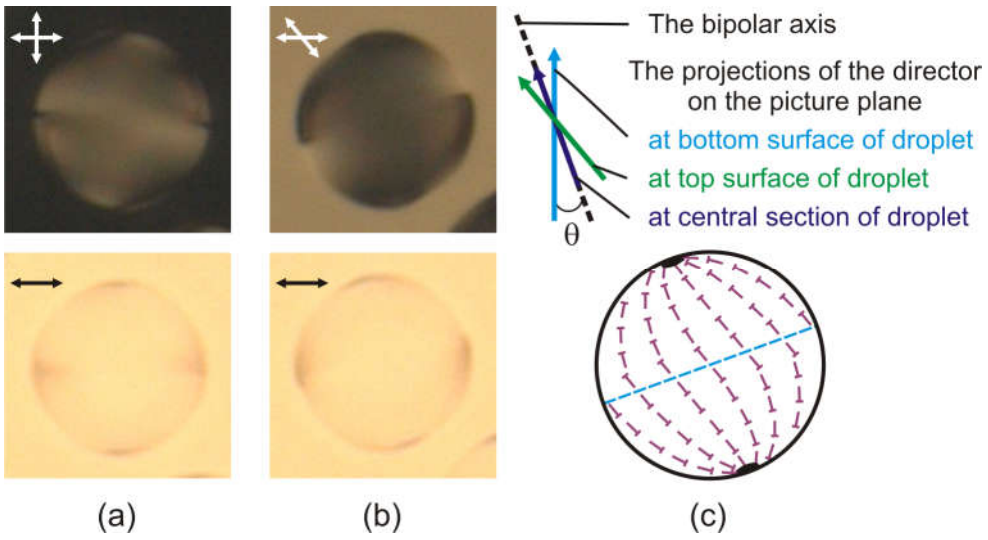

Figure 4. POM images of the LC droplet in crossed polarizers (top row) and without analyzer (bottom row). The bipolar axis of the droplet is perpendicular to the polarizer, the angle between the polarizer and analyzer is 90° (a); the bipolar axis is turned at 20° anticlockwise relative to the polarizer, the angle between the polarizer and analyzer is 130° (b); the scheme of relative orientation of the bipolar axis, the director projection on the picture plane at bottom and top edges (top); the director field over the top droplet surface (bottom) (c). The droplet size is 17 μm.

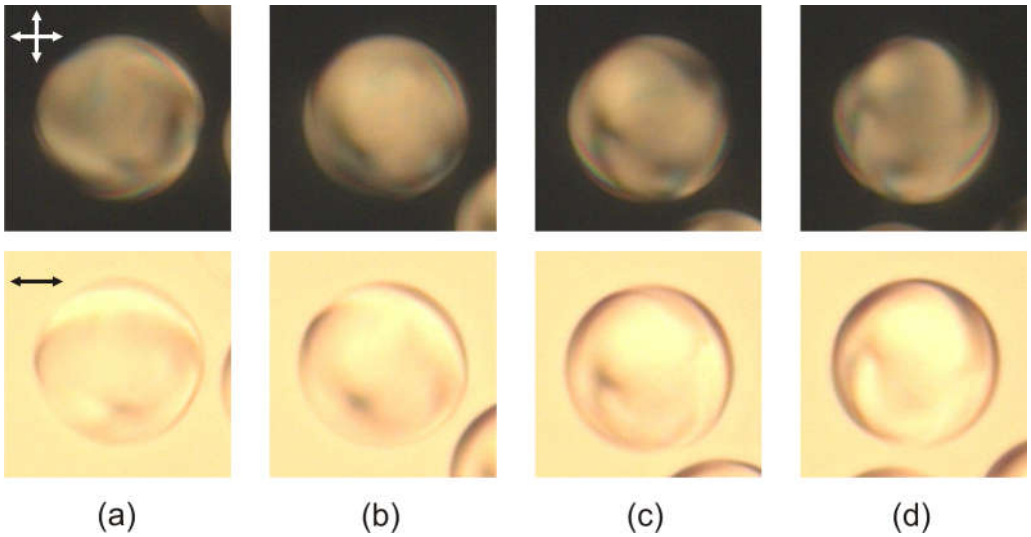

Figure 5. POM images of the LC droplet in crossed polarizers (top row) and without analyzer (bottom row) at the turning angles of microscopic stage 0° (a), 30° (b), 60° (c), 90° (d). The droplet size is 21 μm.

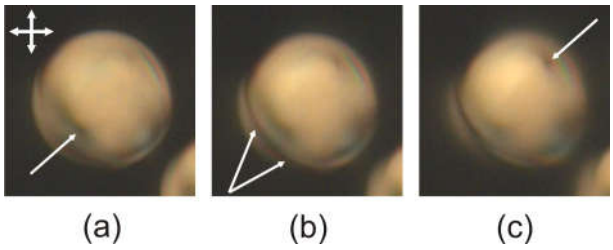

Figure 6. POM images of the LC droplet shown in Figure 5(b) in crossed polarizers. The objective focuses on the bottom defect-boojum (a), the ring defect (b) and top defect-boojum (c). Single arrows indicate the defect positions.

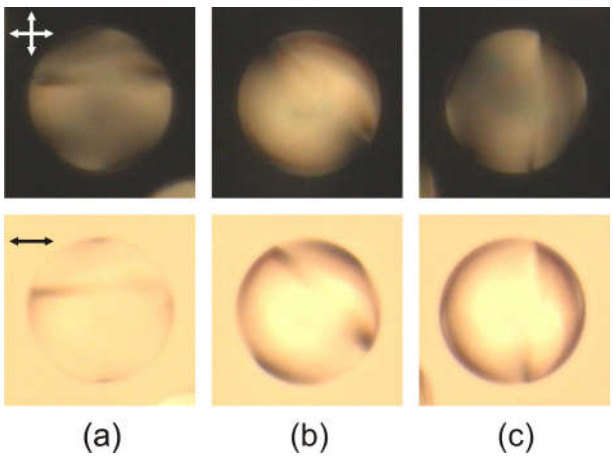

Figure 7. POM images in crossed polarizers (top row) and without analyzer (bottom row). The bipolar axis is orthogonal to the polarizer (a); the sample is turned at 45° clockwise relative to the polarizer (b); the sample is turned at 90° clockwise (c). The droplet size is 23 μm.

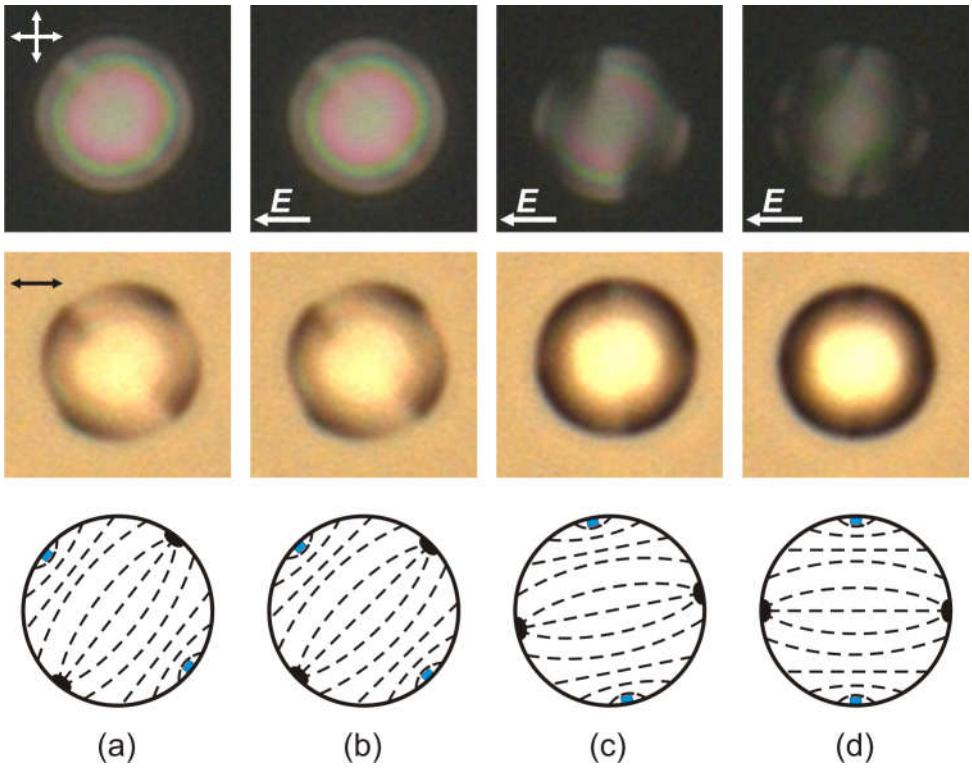

Figure 8. POM images of the LC droplet in the initial state (a), under the 20 V electric field (b), 50 V (c), 90 V (d) made 1 min after switching the electric field on. Images in crossed polarizers (top row), without analyzer (middle row) and the schemes of the proper droplet structures (bottom row). The droplet size is 9 μm. Here and further, a gap between the electrodes is 410 μm, the direction of the electric field ***E*** is shown by a single arrow.

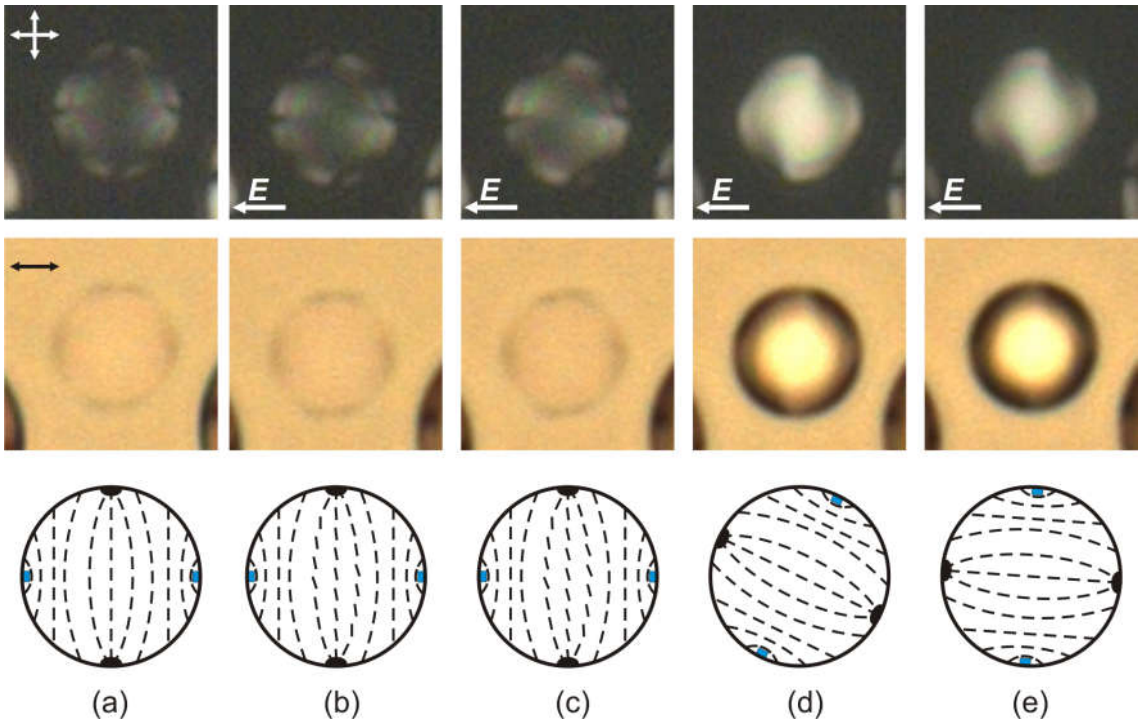

Figure 9. POM images of the LC droplet in the initial state (a) and under the electric field of 40 V (b), 50 V (c), 60 V (d), 90 V (e) made 1 min after switching the electric field on. Images in crossed polarizers (top row), without analyzer (middle row) and the schemes of the proper droplet structures (bottom row). The droplet size is 8 μm.

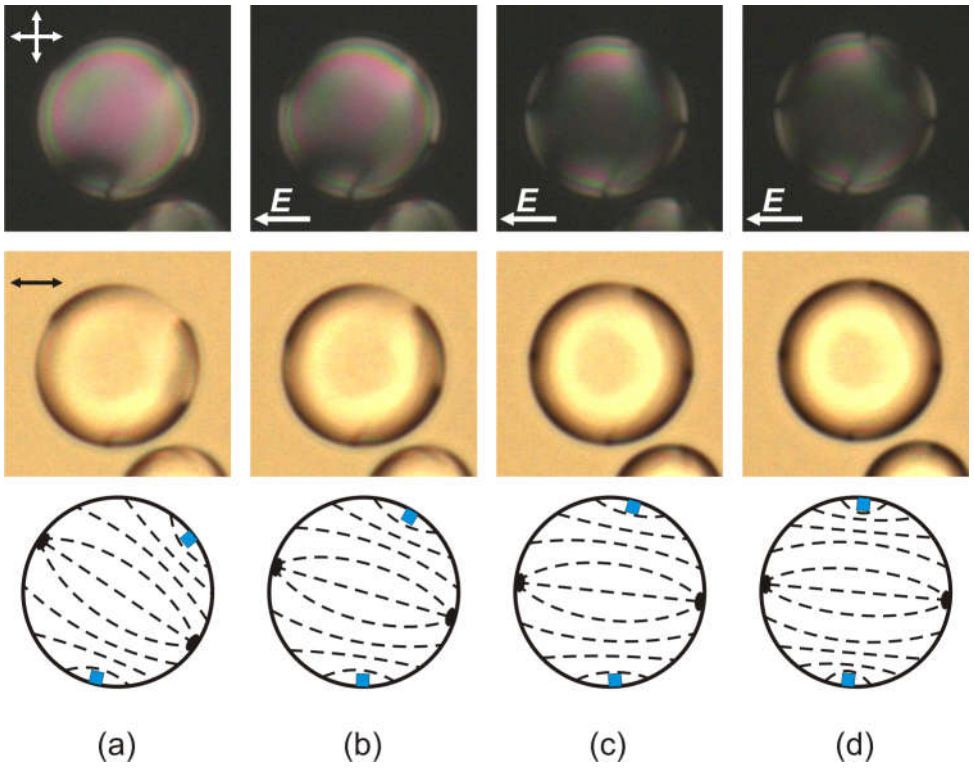

Figure 10. POM images of the LC droplet in the initial state (a) and under the electric field of 20 V (b), 50 V (c), 90 V (d), made 1 min after switching the electric field on. Images in crossed polarizers (top row), without analyzer (middle row) and the schemes of the proper droplet structures (bottom row). The droplet size is 20 μm.